20 years of Hubble Space Telescope optical modeling using Tiny Tim

John E. Krist[a], Richard N. Hook[b], Felix Stoehr[b]
[a]9655 Saluda Ave, Tujunga, CA USA 91042
[b]European Southern Observatory, Karl Schwarzschild Str. 2, D-85748, Garching, Germany

ABSTRACT

Point spread function (PSF) models are critical to Hubble Space Telescope (HST) data analysis. Astronomers unfamiliar with optical simulation techniques need access to PSF models that properly match the conditions of their observations, so any HST modeling software needs to be both easy-to-use and have detailed information on the telescope and instruments. The Tiny Tim PSF simulation software package has been the standard HST modeling software since its release in early 1992. We discuss the evolution of Tiny Tim over the years as new instruments and optical properties have been incorporated. We also demonstrate how Tiny Tim PSF models have been used for HST data analysis. Tiny Tim is freely available from tinytim.stsci.edu.

Keywords: Hubble Space Telescope, point spread function

1. INTRODUCTION

The point spread function (PSF) is the fundamental unit of image formation for an optical system such as a telescope. It encompasses the diffraction from obscurations, which is modified by aberrations, and the scattering from mid-to-high spatial frequency optical errors. Imaging performance is often described in terms of PSF properties, such as resolution and encircled energy. Optical engineering software, including ray tracing and physical optics propagation packages, are employed during the design phase of the system to predict the PSF to ensure that the imaging requirements are met. But once the system is complete and operational, the software is usually packed away and the point spread function considered static, to be described in documentation for reference by the scientist. In this context, an optical engineer runs software to compute PSFs while the user of the optical system simply needs to know its basic characteristics.

For the Hubble Space Telescope (HST), that is definitely not the case. To extract the maximum information out of an observation, even the smallest details of the PSF are important. Some examples include: deconvolving the PSF from an observed image to remove the blurring caused by diffraction and reveal fine structure; convolving a model image by the PSF to compare to an observed one; subtracting the PSF of an unresolved source (star or compact galactic nucleus) to reveal extended structure (a circumstellar disk or host galaxy) that would otherwise be unseen within the halo of diffracted and scattered light; and fitting a PSF to a star image to obtain accurate photometry and astrometry, especially if it is a binary star with blended PSFs

Compared to ground-based telescopes HST is extremely stable, so the structure in its PSF is largely time-invariant. This allows the use of PSF models for data analysis. On the ground, the variable PSF structure due to the atmosphere and thermal-and-gravitationally-induced optical perturbations make it more difficult to produce a model that accurately matches the data. The effective HST PSF, though, is dependent on many parameters, including obscurations, aberrations, pointing errors, system wavelength response, object color, and detector pixel effects. An accurate PSF model must account for all of these, some of which may depend on time (focus, obscuration positions) or on field position within the camera (aberrations, CCD detector charge diffusion, obscuration patterns, geometric distortion).

1.1 Early HST PSF modeling: TIM

Before launch of HST in 1990, a variety of commercial and proprietary software packages were used to compute PSFs. These provided predictions of HST's imaging performance and guided the design, but they were not used by future HST observers. These programs were too complicated for general HST users, and either were not publicly available or were too expensive. They also did not provide PSF models in forms that scientists would find useful, such as including the effects of detector pixelization and broadband system responses.

Optical Modeling and Performance Predictions V, edited by Mark A. Kahan, Proc. of SPIE Vol. 8127, 81270J · © 2011 SPIE · CCC code: 0277-786X/11/$18 · doi: 10.1117/12.892762

In the latter half of the 1980s at the Space Telescope Science Institute (STScI), Christopher Burrows and Hashima Hasan developed TIM[1] (Telescope Imaging Modeling), a program written to compute HST PSFs for image simulations prior to launch. TIM, up to its final release, included effects such as: integration of the image onto finite area detector pixels; measured optical surface maps of the primary and secondary mirrors; field dependent obscuration patterns in the HST WF/PC-1 and WFPC2 cameras, based on relations derived from ray tracing using other programs; large angle scattering from optical microroughness and dust, implemented as an analytical modification to the system modulation transfer function; jitter (pointing errors during an exposure) modeled as a convolution with a Gaussian of some specified width; and optional addition of cosmic rays and Poisson and read noise.

Up to the release of Tiny Tim in 1992, TIM was the primary HST PSF simulation tool used by astronomers to plan and analyze their observations. However, as the importance of using PSFs for deconvolution became critical after the discovery of spherical aberration in HST, the implementation constraints of TIM limited its use by the community. It had a somewhat steep learning curve, initially requiring answering nearly 80 questions during each execution (this was later alleviated by a wrapper routine that reduced the number of queries). Its main limitation, though, was a lack of portability. Written in Fortran, it made use of vendor-specific language extensions that allowed it to be compiled and run only on VAX VMS systems (and not on the later Alpha processor VMS computers). It thus could not make use of faster UNIX workstations that became available in the early 1990s. Updates to TIM stopped in the late 1990s.

2. TINY TIM

2.1 Development

To provide a more readily accessible and faster means of generating HST PSFs, development on Tiny Tim began in 1991 by J. Krist. The program's name is something of an homage to TIM, but while Tiny Tim uses some of the same computational techniques as TIM, is was developed from scratch and contains no code derived from its predecessor. Tiny Tim is written in standard C and is self-contained (including FFT and FITS file routines), so the user does not need to download additional libraries. It also makes use of C's dynamic memory allocation to allow for grid sizes that are appropriate for the instrumental setup (TIM had fixed-sized grids determined at compile time). Multithreading has also been added to some routines (interpolation and geometric distortion) in recent years to speed execution on multi-CPU systems.

The first public release of Tiny Tim was in January 1992. It has always been freely available for download from STScI via ftp or the Institute's web site (tinytim.stsci.edu). It is distributed as source code that the user compiles on their own UNIX or Mac OS system by running a single **make** command. The distribution includes a library of properties for each camera (wavelength range, field position, detector pixel size, etc.) and filter transmission curves, as well as spectra for selected stellar types (O through M).

2.2 Program execution

Tiny Tim has two basic programs. The first, **tiny1**, asks the user a basic set of questions that define the observation:

- Instrument to model
- Diameter of the PSF in arcseconds
- Subsampling relative to the default pixel scale (optional)
- Detector coordinates (for those instruments with known field dependent aberrations or obscurations)
- Filter (the filename of a user-supplied system transmission table may be used)
- Stellar spectral type (from a list of selected types, or the filename of a user-supplied spectrum may be used)
- Date of observation (for some instruments), which sets the time-dependent aberrations

Based on the specified PSF diameter and wavelength range of the filter, **tiny1** will determine the appropriate computational grid sizes to use. It multiplies the filter curve by the chosen stellar spectrum; the curve consists of transmission values at a sufficient number of wavelengths to sample the bandpass (15-25 for broad bandpasses). The results, along with the default instrument parameters and aberrations, are written to a plain text parameter file the user may edit this file prior to running the next stage to modify the aberration values or turn off certain features if necessary.

The next program, **tiny2**, reads in the parameter file and computes the PSF. For a polychromatic PSF, it generates separate monochromatic PSFs at the wavelengths specified by the filter curve and then adds them together, weighted by the system transmission and object spectrum.

A third program, **tiny3**, performs geometric distortion of ACS and WFC3 camera PSFs, as will be described later.

2.3 Web interface

A web-based interface[2] to Tiny Tim was recently developed at the Space Telescope European Coordinating Facility, coeval with the addition of the Wide Field Camera 3. The interface simplifies the choices to drop-down menus, and computes the PSF on the web server itself. The service is now hosted at STScI at tinytim.stsci.edu. Recent modifications to Tiny Tim include the option to input time-dependent focus obtained from a separate web-based focus model.

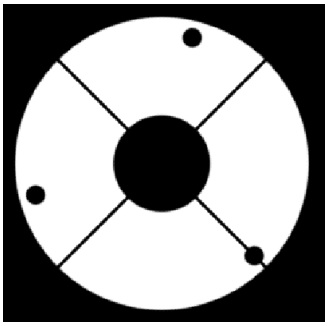

Figure 1. The HST obscuration pattern (excluding any obscurations from the cameras). The three small circles are pads that hold the primary mirror in place.

3. MODELING THE HST PSF

3.1 Diffraction calculation

Tiny Tim performs the most simplistic diffraction calculation. It assumes that all of the aberrations and obscurations in a system are projected onto the entrance pupil that is propagated to focus using a single Fast Fourier Transform (FFT). Fresnel effects from optic-to-optic propagation are not included. Only for the WF/PC-1 and WFPC2 cameras, which have obscurations not in a pupil plane, would accounting for the Fresnel effects improve the PSF accuracy. However, PSF errors due to unknown or poorly known parameters, such as time dependent aberrations, dominate over any Fresnel effects.

An $n \times n$ element array is used to represent the wavefront. The pupil occupies half the diameter of this grid, resulting in a PSF that is Nyquist sampled (0.5 λ/D radians/pixel, where D is the entrance diameter). The value of n is computed based on the requested PSF size and the wavelength. After the array is propagated to focus with an FFT, the square of the absolute value of the complex-valued electric field is taken to produce the PSF.

3.2 Obscurations

The Hubble telescope obscurations (Figure 1) are the primary mirror edge, the secondary mirror and support spiders, and three circular pads that hold the primary in place. The WF/PC-1, WFPC2, NICMOS, STIS-CCD, ACS/HRC coronagraph and WFC3-IR cameras also had/have internal obscurations that are projected onto the entrance pupil. Obscurations are drawn into the wavefront grid with antialiased edges (the pixel value varies from 0 to 1 depending on the fraction of the pixel area covered by the obscuration).

3.3 Aberrations

Low order aberrations are included by Tiny Tim using up to 22 Zernike polynomials (up to 5th order spherical) normalized for a 33% central obscuration. The telescope and camera aberrations are projected onto the entrance pupil. The polynomial coefficients are stored in the parameter file produced by **tiny2** and represent the aberrations measured at the center of the detector. They can be adjusted if the user wants to try to optimize the PSF to a particular observation and filter. The default aberrations were derived from model-fitting phase retrieval of on-orbit star images[3].

All of the cameras exhibit field dependence of aberrations, mostly focus, coma, and astigmatism. In some cameras these variations have been measured via phase retrieval (or, for WFC3, predicted from ray tracing the prescription[2]), and 2-D polynomial relations have been established. Given detector coordinates, Tiny Tim will use these relations to compute the offsets in aberration values from the default field-center ones.

Defocus

Despite being in space, HST experiences time-and-attitude-dependent aberration changes[4,5]. Since being placed in orbit, the telescope has desorbed water from its graphite epoxy truss, causing it to shrink exponentially over time by about 150 microns. Left alone, these changes would have introduced nearly two waves RMS (@ λ=500 nm) of defocus as the separation between the primary and secondary mirrors decreased. To compensate, the secondary mirror has occasionally been moved away from the primary, usually by a few microns. In the first two years moves were done frequently, but since 2000 they have occurred about once every two years. Tiny Tim has a database of dates of mirror moves and measured focus values at those times for the 1990-1993 period when HST was uncorrected. For the aberrated cameras (WF/PC-1, FOC), the user-specified date is used by **tiny1** to look up the focus at the closest previous move and then more defocus is added to account for desorption that occurred since then (characterized by an exponential curve fit to focus monitoring data). Tiny Tim does not store time-dependent focus information for the corrected cameras (except NICMOS, as described later), so the user is not asked for an observation date when modeling them. Focus changes can, however, be included to optimize PSF matches to the data, as detailed below.

While desorption causes long-term changes in focus, another effect, *breathing*, occurs on orbital timescales. HST can continuously point at a target over many orbits, and for most pointings the Earth will pass in front of the telescope once per orbit. The heat of the planet entering the telescope causes the truss to expand, changing focus. Once the Earth passes, the truss cools and shrinks and the focus change reverses. The truss length typically cycles by about 3 microns during an orbit, causing a focus change of ~18 nm RMS. Another heating effect is related to the attitude of the telescope relative to the Sun and can cause larger focus excursions, by as much as 60 nm RMS when HST is pointed opposite to the Sun for multiple orbits. A new feature has recently been developed by STScI to estimate the focus[6] in a particular camera for a given observation date and time. The web-based model (http://www.stsci.edu/hst/observatory/focus/FocusModel) uses engineering telemetry containing temperature information, historical temperature trends, and the measured long-term focus trends to compute the appropriate focus due to breathing and desorption for any time during a visit. The result is expressed in terms of a equivalent secondary mirror defocus offset. Tiny Tim v7.0 or later (including the web interface) will ask if the user want to enter this value. Any field-dependent defocus offsets are added to this value by **tiny2** based on the specified detector position.

Polishing errors

Even the best polishing processes leave surface errors on optics that scatter light into the wings of the PSF. On the ground these effects are usually not a dominant factor, given that the halo of scattered light from atmospheric turbulence is much larger. However, on HST scattered light from the primary and secondary mirror surface errors dominates over diffraction in the PSF wings beyond an arcsecond or so in the visible, and even closer to the star in the ultraviolet. The scattering halo is filled with speckles that, when viewed over a broad bandpass, smear into streaks radiating from the star. When looking for faint objects near a star (low-mass companions or circumstellar disks, for instance), these speckles create a complex background against which detection can be difficult. In crowded stellar fields, such as globular clusters, the PSF wings overlap, increasing the instrumental background.

Prior to 1995, Tiny Tim included surface error maps of the primary and secondary mirrors obtained from pre-launch interferometer measurements. It was clear that they were not sufficiently accurate to duplicate the fine-scale structure in the PSF wings. After installation of the corrective optics in WFPC2 in 1993, phase retrieval[3] was used on highly-defocused star images to derive a new error map (Figure 2). The retrieved map more clearly reveals mid-spatial-frequency errors in the optics. Depending on the focal plane location of the camera, the beam from the primary mirror falls on different regions of the secondary, an effect that is taken into account. The new map was obtained from WFPC2 PC data and represents the projection of all the optical errors onto the entrance pupil as seen by the PC. The pre-launch secondary mirror map was subtracted from the retrieved map to provide a new primary map. Tiny Tim reads in the new primary map and pre-launch secondary map, shifts the secondary map via interpolation as appropriate for the field location of the selected camera, and adds them together. The improvement in agreement between model and data due to the new map is great, especially at shorter wavelengths (Figure 3).

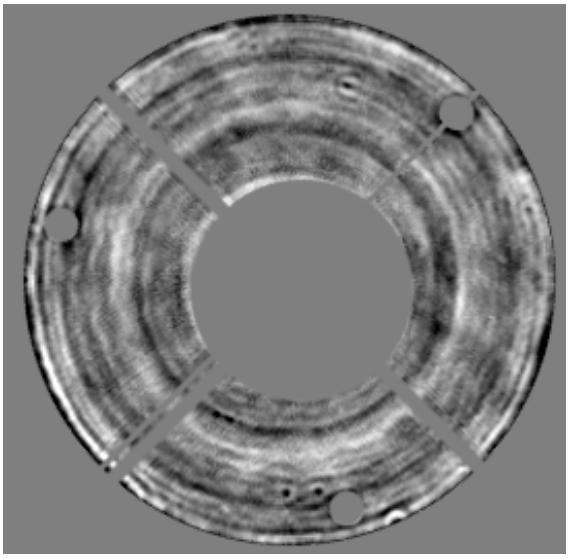

Figure 2. Map of the combined primary and secondary mirror surface errors left from polishing obtained using phase retrieval on highly defocused star images. Shown between ±30 nm surface error. The HST and WFPC2 obscuration patterns are superposed.

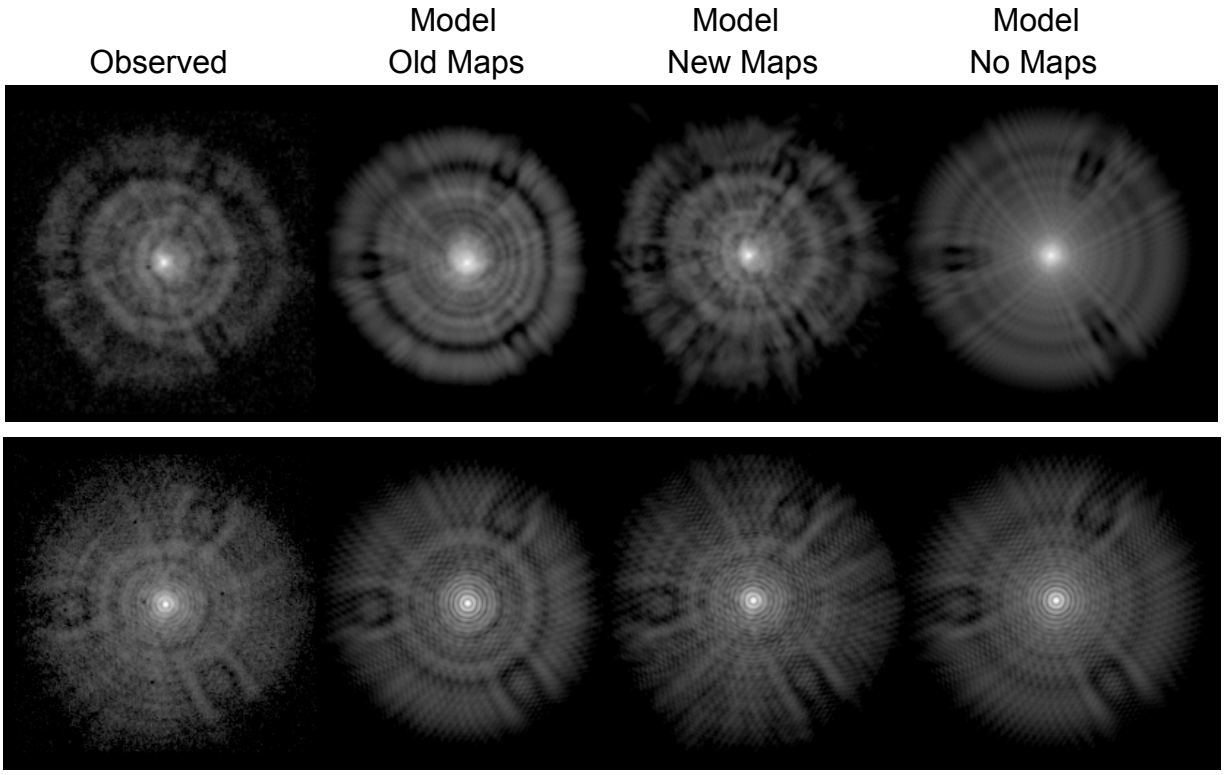

Figure 3. Spherically-aberrated observed and simulated PSFs from the Faint Object Camera using (top) filter F253M (253 nm central wavelength) and (bottom) filter F486N. The models were generated using the old (pre-launch) optical surface error maps, the new maps from phase retrieval, and no surface error maps. Each PSF is approximately 6 arcseconds in diameter. The three lobes are shadows from the primary mirror restraining pads.

3.4 Jitter

HST uses its gyroscopes and Fine Guidance Sensors to maintain pointing on the target during observations. Motion is controlled by reaction wheels. The mean time-integrated pointing error function (jitter) is roughly Gaussian with an RMS width of 3 milliarcseconds. Prior to pointing optimization that occurred a couple years after launch, the accuracy was ~7 mas. Jitter is modeled as a Gaussian blur with a user-specified RMS. The default shape is symmetrical jitter, but elliptical jitter can be specified. In most cases, jitter is not a significant factor and so the default is to not include any.

3.5 Pixel integration

While Tiny Tim does not perform full surface-to-surface propagation like some optical design packages, it does something very important that is usually left out of those programs – pixelization. The Nyquist sampled PSF produced as an intermediate product by **tiny2** consists of values at infinitely small points. To match the model to what is seen on the detector, the PSF must be integrated onto the finite-width pixels. The HST PSF has a large amount of high spatial frequency content, including the sharp core and speckles and streaks in the wings. The PSF intensity can vary considerably over the area of a pixel, especially if the detector is undersampled (i.e., samples at lower than the Nyquist spatial frequency criterion of $F\lambda/2$, where F is the focal ratio). The WFPC2 WF cameras, for example, undersampled the PSF by 7× at λ = 336 nm, and the PSF core width was smaller than a pixel (Figure 4). The large majority of HST observations have been done using undersampled cameras.

Pixel integration is accomplished by convolution of the point-sampled PSF with the pixel area: the Fourier transform of the Nyquist sampled PSF is computed via FFT, then multiplied by the analytic transform of a rectangular pixel (a sinc function), and inverse Fourier transformed. The result has values that represent the intensity over detector-sized pixels but at Nyquist spacing. Damped (Lanczos) sinc interpolation is used to obtain values at detector pixel spacing. This is done for each monochromatic PSF. Note that at the stage where the Fourier transform of the PSF is available, it is also multiplied by a Gaussian representing the analytic transform of the jitter function (if any jitter is specified).

The ability to sample with arbitrary fineness is a distinct advantage of model PSFs. Because of the high spatial frequency content in the PSF, the appearance of an unresolved source, especially in the PSF core, is highly dependent on centering of the source within a pixel. A subsampled model can be generated, interpolated to shift its center relative to the detector pixels, and rebinned to normal sampling. This is especially important for PSF fitting photometry and astrometry.

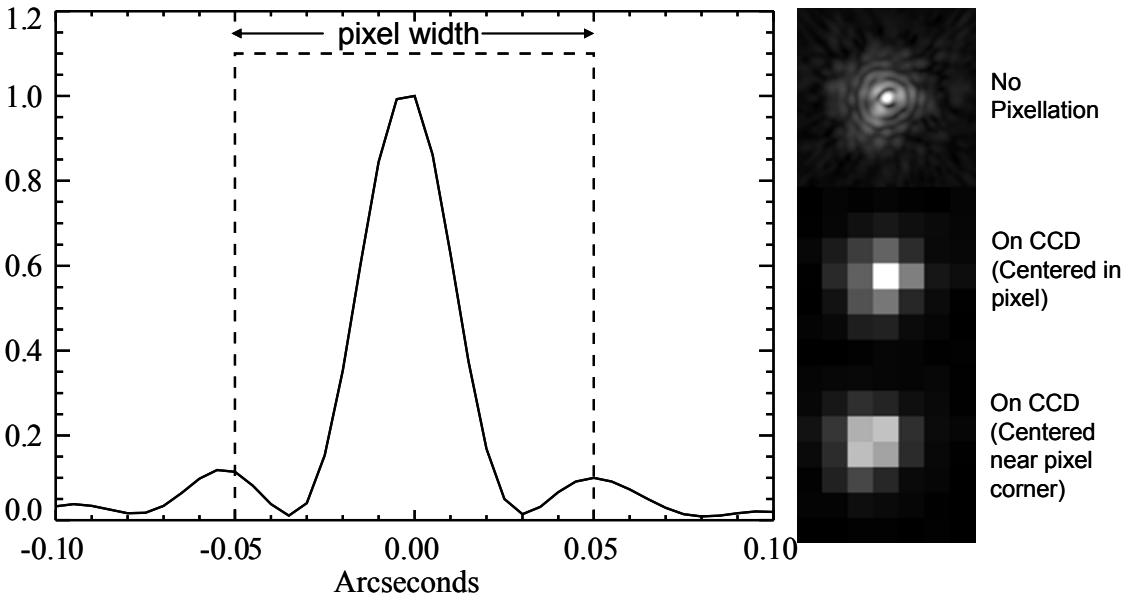

Figure 4. (Left) Cross-section through a computed HST PSF at λ = 336 nm. The width of a WFPC2 WF pixel (0.1") is shown. (Right) On top, the computed 336 nm HST PSF prior to pixellation. Below it is the PSF centered at the middle of a pixel and in the corner, integrated over the WFPC2 WF pixel area, shown at the same spatial scale.

4. SIMULATION OF ABERRATED (PRE-CORRECTION) CAMERA PSFS

HST suffers from 0.25 μm RMS of spherical aberration caused by an improperly figured primary mirror, preventing the telescope from achieving proper focus[7]. Prior to the 1st servicing mission in December 1993, when corrective optics were installed, HST was set to be near paraxial focus, so that rays from the center of the primary were in focus but those from the outer (marginal) regions of the mirror were not. This resulted in a narrow core containing about 15% of the light with wings extending to ~3 arcseconds containing the remainder (Figure 3). The wings of the PSF were essentially defocused, and the shadows of the obscurations (spider vanes, primary mirror pads) were visible as tendrils extending from the core.

These effects of spherical aberration impacted the effective resolution of the telescope to some extent, but mostly they diminished contrast by distributing light into the field. In compact star fields such as globular clusters, the wings of the PSFs would overlap, creating a high background. Because of the structure in the wings, fainter sources were difficult to identify. Features in galaxies, nebulae, and planets were washed out. The tight core would allow bright, sharp features to be identified, but fainter, extended components (spiral arms in galaxies, planetary surface features) would be diminished.

During the ~3.5 years HST images were aberrated, deconvolution was used to restore some image resolution and contrast. The deconvolution algorithms required knowledge of the point spread function; many of them functioned by creating an unaberrated model of the field that was convolved with a provided PSF and then compared to the observed, aberrated image; the model image was iteratively refined until agreement was achieved. High signal-to-noise PSFs taken in the same filter and at the same field position as the observation were rare. The choice was to use an observed stellar PSF taken in an non-optimal instrumental configuration, spend precious observing time taking images of reference stars, or use simulated PSFs.

4.1 Wide Field/Planetary Camera (WF/PC-1)

WF/PC-1 was composed of four wide-field (WF:f/12.9, 0.1”/pixel) and four high-resolution, “planetary” (PC:f/30.0, 0.043”/pixel) channels. The field at the HST focus was split into four channels using a pyramid mirror that could be rotated to select between the WF and PC cameras. Each channel had a Cassegrain repeater optic to reimage the focal plane onto a 800 × 800 pixel CCD (eight repeaters and eight CCDs in all). It operated over a $\lambda = 120 – 1100$ nm range with a large selection of narrow, medium, and wide-band filters.

Because the repeater secondary mirror and supports were not in a pupil plane, the obscurations appeared to shift relative to the telescope’s depending on field position. The effect of this shifting was pronounced WF/PC-1 because of the spherical aberration, which caused “shadows” of the camera obscurations and the telescope mirror support pads (Figure 5). The increased beam size at the repeater entrance baffles due to the spherical aberration also caused vignetting at the edges of the field in the WF channels that would clip the edges of the PSFs. These variations made deconvolution difficult, since the positions of the shadows in the wings could change significantly with field offsets of only tens of pixels. The resulting mismatches would lead to residuals in the wings of the restored PSFs. Since Tiny Tim models can be generated for any position, an optimum PSF can be used for wherever the object is on the detector.

WF/PC-1 was known to have field dependent aberrations (focus, coma, and astigmatism), but they were not well characterized. The aberrations for the center of the field in each channel, measured by phase retrieval, are used for all field positions in Tiny Tim. WF/PC-1 also suffered from geometric distortion, which is not modeled. CCD charge diffusion is also not included, but its blurring effect was not noticeable due to the blurring caused by spherical aberration.

4.2 Faint Object Camera (FOC)

The FOC was optimized for ultraviolet observations over a wavelength range of $\lambda = 115 – 600$ nm with a selection of narrow, medium, and wide-band filters. It had two channels, f/48 (0.045”/pixel) and f/96 (0.022”/pixel). The f/48 channel was rarely used. Each had a 512 × 512 pixel photocathode tube detector. The readout could be adjusted to provide 1024 × 512 pixels, but only with 8 bits/pixel dynamic range (Tiny Tim only models the default 512 × 512 modes). The images produced by the FOC were highly distorted due to the nature of the photon counting detectors. Most of the distortion was corrected in the calibrated data, but near the field edges it was still fairly high. Tiny Tim assumes there is no distortion. There were also some field dependences of the aberrations, but they were small and not well characterized and are not included in Tiny Tim FOC models. The Corrective Optics Space Telescope Axial Replacement (COSTAR) assembly, installed in 1993, included optics that corrected the HST spherical aberration for FOC.

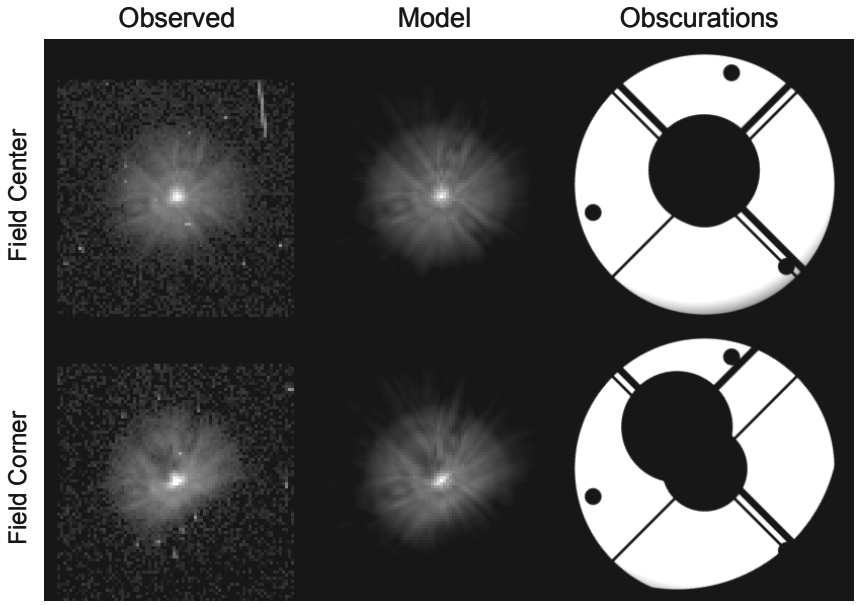

Figure 5. (Left) Images of a star observed using the aberrated WF/PC-1 WF camera (channel 2) and filter F555W (cosmic ray trails are visible). The star was positioned at the center (top row) and extreme upper left corner (bottom row) of the detector. (Middle) Tiny Tim model PSFs generated for the same detector position. (Right) The corresponding obscuration patterns generated and used by Tiny Tim to create the models. The WF/PC-1 internal obscurations are seen (3-vaned spider, larger secondary mirror shadow, and vignetting baffle aperture at the lower right edge of the pupil).

5. SIMULATION OF 2ND GENERATION CAMERA PSFS

The installation of WFPC2 and COSTAR during Servicing Mission 1 in December 1993 successfully corrected the spherical aberration in the telescope, restoring its effective optical performance to the design specifications.

5.1 Wide Field and Planetary Camera 2 (WFPC2)

WFPC2 was originally to be a copy of WF/PC-1 but with improved detectors. After the discovery of HST's spherical aberration, its design was changed to incorporate corrective optics. Instead of WF/PC-1's four WF and four PC channels selected with a rotating pyramid mirror, WFPC2 had one PC (f/28.3, 0.0456"/pixel) and three WF (f/12.9, 0.1"/pixel) channels with a fixed pyramid. Like WF/PC-1, though, each channel used a small Cassegrain repeater that created a field-dependent obscuration pattern. The aberration correction was done by the repeater, meaning no additional optics were required.

Some WFPC2 aberrations (focus, coma, astigmatism) varied with field position. Jon Holtzman (New Mexico State University) provided relations for these derived from PSF model fitting that are used by Tiny Tim. The user-specified detector position of an observation is used to compute both the obscuration pattern and aberrations. Geometrical distortion is not included in the simulations. The WFPC2 filters had small but different amounts of optical wedge that caused tiny shifts of the beam in the repeater. This introduced differing amounts of coma between filters, but this effect was not accurately measured and has not been included in Tiny Tim.

At the extreme red end of the detector bandpass, scattering within the CCD backing substrate created an additional halo of light in the wings of the WFPC2 PSF in filter F1042M. An empirical, radially-symmetric model of the halo is added to model PSFs for that filter. Additional large-angle scattering at all wavelengths was also seen around bright stars. This was produced by light reflected by the matte surface of the front-illuminated CCDs up to the optics and back to the detector. Because of the complexity of this halo, it has not been included in Tiny Tim.

WFPC2 CCD charge diffusion

All CCDs suffer from an effect called charge diffusion, but on HST it was first noticed in WFPC2. CCD pixels are not physically separate elements; they are defined by the electric fields created by the electrode structure. When a photon is converted to an electron in the substrate, the electron tends to be attracted to the nearest electrode. But in regions where the field strength is weak (i.e. furthest from the electrode), an electron may travel some distance from where it was generated, even into an adjacent pixel (hence the term charge diffusion). The net effect is blurring of the image.

The amount of charge diffusion varies with wavelength. Shorter wavelength photons are converted to electrons near the illuminated surface of the detector, while longer wavelength ones typically require a longer path (very long wavelength light can actually pass through the substrate without being detected). In backside illuminated CCDs (like in WF/PC-1, STIS, ACS, and WFC3), the electrodes are on the rear side of the detector, closer to where long wavelength photons are converted. Thus, in such devices charge diffusion becomes worse with decreasing wavelength. For front-side illuminated CCDs, like those used in WFPC2, the opposite is *not* true. Charge diffusion is high at longer wavelengths (>800 nm), but also at shorter ones (<400 nm), since the short wavelength photons are scattered by the electrode structure on the illuminated surface. Charge diffusion is lowest at about 550 nm.

Charge diffusion in WFPC2 slightly blurred its images, producing an effect similar to pointing jitter. In the PC it was equivalent to about 14 milliarcseconds RMS of jitter, while in the WFs, because they largely undersampled the PSF, the effect was more like 40 mas. The wavelength dependence of the WFPC2 charge diffusion function was not characterized. Tiny Tim approximates the effects of charge diffusion by convolving the normally sampled PSF by a 3 × 3 pixel Gaussian kernel. This kernel is most appropriate in the range of 500 – 600 nm, but since nothing better is available, it is used at all wavelengths. Because this effect occurs at the pixel level, this charge diffusion kernel is not applied to subsampled PSFs - the user must apply the kernel after rebinning the subsampled PSF to normal sampling. Lauer[8] describes in further detail the charge diffusion characteristics of WFPC2.

5.2 COSTAR-corrected FOC

COSTAR consisted of deployable arms that placed corrective optics in front of the entrance apertures to the High Resolution Spectrograph, Faint Object Spectrograph, and the FOC. It replaced the High Speed Photometer in the HST instrument bay. The optics increased the effective focal length of the FOC cameras (f/96 to f/151, f/48 to f/72.5). Tiny Tim includes COSTAR+FOC aberrations measured at the center of the field.

6. SIMULATION OF 3RD GENERATION CAMERA PSFS

The 2nd servicing mission in February 1997 replaced the two spectrographs with a near-infrared camera and a new spectrograph/camera.

6.1 Near-Infrared Camera and Multi-Object Spectrometer (NICMOS)

NICMOS had three separate channels (NIC1:f/80, NIC2:f/45, NIC3:f/17.2), each containing a 256 × 256 HgCdTe detector. It operated over a $\lambda = 0.8 - 2.5$ μm passband with a variety of narrow, medium, and broad filters. An unexpected expansion of the frozen nitrogen coolant on-orbit caused deformation of the dewar, resulting in misalignments within the optical systems. The three cameras were no longer confocal, with NIC3 pushed beyond the range of the Pupil Alignment Mirror (PAM) that also provided internal focus adjustment. The PAM position was set to optimize focus for NIC1 or NIC2, depending on which was the primary camera. It was also adjusted a number of times from 1997-1998 to track the changes in focus as the dewar deformation continued to move the detectors. The deformation caused the internal cold pupil stops, which masked the warm HST obscurations, to become misaligned and drift, creating a time-dependent obscuration pattern. To allow NIC3 observations, two three-week periods in 1998 were dedicated to that camera, with the HST secondary mirror moved to bring it into the adjustment range of the PAM (all other HST instruments were out of focus during these times). After the coolant ran out in January 1999, NICMOS observations stopped until June 2002, after the NICMOS Cooling System (NCS) cryocooler was installed during the 3rd servicing mission. With the NCS, the system was stable and an intermediate focus position was chosen for NIC1 and NIC2 (NIC3 remained out of focus). NICMOS continued to operate until September 2008, when the NCS failed.

The initial implementation of NICMOS in Tiny Tim was undertaken at the Space Telescope European Coordinating Facility by R. Hook.[9]

NICMOS had a coronagraphic mode in NIC2 using a 0.3" radius hole drilled in a focal plane mirror as the occulter and the cold stop as the Lyot stop. Tiny Tim does not model this mode. Nor does Tiny Tim include the NICMOS detector subpixel response variations - the effects were largely confined to the undersampled and rarely used NIC3 camera.

For the pre-NCS era, Tiny Tim has a table of phase-retrieval-measured NICMOS aberrations (focus, coma, astigmatism, trefoil, spherical) corresponding to the dates of the PAM adjustments. This is used for the date of observation specified by the user. For NICMOS+NCS, constant aberrations are assumed for each camera (measured using phase retrieval), though the user is asked whether the observation occurred after May 16, 2002, when a coma adjustment was made using an internal mechanism. Focus, coma, and astigmatism varied in the NICMOS cameras with field position. In cameras 1 and 2 focus varied linearly across the field, while in camera 3 it varied quadratically, with the best focus at the center. These variations were measured using phase retrieval. Tiny Tim includes these variations.

Each NICMOS camera has a cold stop located at a pupil that masks the warm HST obscurations. The dewar deformation caused these stops to be misaligned with respect to the optical axis (by about 12% of the pupil radius in NIC1 and NIC2, 5% in NIC3). Their X,Y offsets were derived via phase retrieval, which was routinely used for focus monitoring. In NIC2 the mask drifted by about 2% of the pupil radius between 1997-1998. The resulting asymmetrical pupil caused diffraction rings to appear elliptical. A table of the NIC2 cold mask offsets over time is included in Tiny Tim and is used for the pre-NCS era observations. The appropriate position is used based on the date entered by the user. Constant offsets are used for the NIC1 and NIC3 cold masks, as those were not continually measured over time like NIC2. For the NCS era, constant offsets are used.

6.2 Space Telescope Imaging Spectrograph (STIS)

STIS is an imager/spectrograph with three selectable channels: an optical (λ = 250 – 1000 nm) 1024 × 1024 pixel CCD (f/35.5, 0.051"/pix), a near-UV (λ = 160 – 310 nm) MAMA (f/86.9, 0.025"/pix), and a far-UV (λ = 115 – 170 nm) MAMA (f/86.9, 0.025"/pix). As the primary purpose of STIS is spectroscopy, there are a very limited number of filters. The CCD has two narrow band and one long-pass (λ = 530 – 1000 nm) filters, plus an unfiltered setting for imaging over the full CCD bandpass (this is the only mode for coronagraphic imaging). The unfiltered mode requires 107 monochromatic PSFs to be generated to create a broadband PSF. Most imaging with STIS has been in the coronagraphic mode.

The STIS optical system has not been thoroughly characterized, so Tiny Tim uses the same aberrations (based on phase retrieval measurements at field center) for all three channels. Field dependent aberrations are not included. STIS is optimized for spectroscopy, so the system is set for best focus at the slit. The CCD and MAMA imaging modes are thus very slightly out of focus, which is accounted for by Tiny Tim.

Wavelength dependent image blurring caused by CCD pixel charge diffusion is included using the ACS HRC field-center values (which is the same type of detector used by STIS). Field dependent charge diffusion is not modeled. At wavelengths >600 nm, the CCD becomes partially transparent, allowing red photons to pass through the detector, scatter within the backing substrate, and wander back up into the detector at large angles from their incident location. This effect creates a "red halo" that increases with wavelength. The halo has structure and has not been well characterized, so it is not included by Tiny Tim. The STIS NUV MAMA also has a halo caused by a different form of charge diffusion, which is also not modeled by Tiny Tim.

The CCD mode includes a Lyot stop that is always in place and masks only the outer edge of the pupil. Because the stop is not located exactly in a plane conjugate to the exit pupil, its location relative to the OTA pupil appears to shift with field position. Tiny Tim assumes that the stop does not shift and is always at the position appropriate for the center of the field (the mask is slightly misaligned at this location, and this is accounted for by Tiny Tim). Due to the angle of incidence of the beam on the mirror, the projection of the Lyot stop on the pupil appears slightly elliptical.

7. SIMULATION OF LATER GENERATION CAMERA PSFS

The Advanced Camera for Surveys was installed during the 4th servicing mission (SM3B) in March 2002, along with the NICMOS Cooling System. In the final servicing mission (SM4) in May 2009, the Wide Field Camera 3 (WFC3) and Cosmic Origins Spectrograph were installed, replacing WFPC2 and COSTAR (Tiny Tim does not model COS).

7.1 Advanced Camera for Surveys (ACS)

ACS is composed of three channels. The wide field channel (WFC:f/26, 0.05"/pixel) has two 4096 × 2048 CCD detectors for λ = 400 – 1100 nm imaging. The high resolution channel (HRC:f/72, 0.025"/pixel) has a single 1024 × 1024 CCD for λ = 170 – 1000 nm imaging. The solar blind channel (SBC:f/72, 0.030"/pixel) uses a STIS-like MAMA detector for λ = 115 – 170 nm imaging, and it shares the HRC optical train and field of view (an actuated mirror selects the detector). WFC and HRC/SBC image separate portions of the HST focal plane. The HRC is no longer in operation due to an electronic failure. That channel also had a selectable coronagraphic mode (occulted sources are not simulated by Tiny Tim, though field sources are by including the Lyot stop in the obscuration pattern).

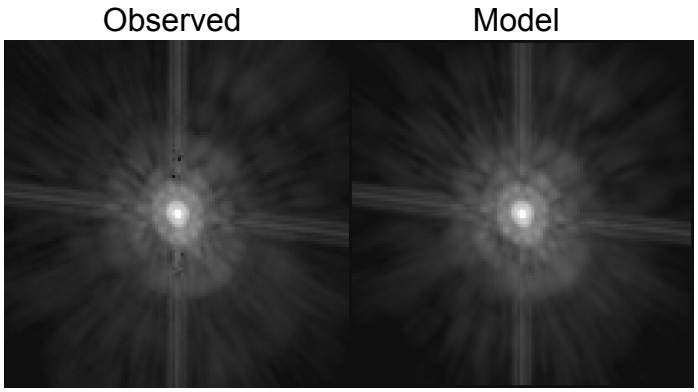

Figure 6. Observed (left) and Tiny Tim model (right) ACS HRC PSFs (filter F555W). The images have not been distortion corrected, so the diffraction spikes do not appear perpendicular to each other.

Geometric distortion

ACS is located away from the optical axis of HST, so it suffers from significant distortion (Figure 6) that is not corrected by the internal optics. The projection of the camera's field-of-view onto the sky looks like a sheared rectangle – the distance along one diagonal is greater than the other. Because of this effect, it is not sufficient for Tiny Tim to generate undistorted PSFs for ACS like it does for the other cameras.

When simulating ACS, **tiny2** will produce an intermediate, undistorted PSF that is sampled 1.3× better than Nyquist at the shortest wavelength in the passband (no charge diffusion is included at this stage). A third program, **tiny3**, reads this in and performs the distortion. Each distorted pixel in the output image is divided into subpixels (the more undersampled the PSF is on the detector, the more subpixels are used). For each subpixel, the corresponding value in the undistorted **tiny2** PSF is retrieved via interpolation, and all of the subpixels are then added together. The distorted image is then convolved with the charge diffusion kernel (detailed later). **tiny3** also provides the ability to generate geometrically distorted star fields. The user provides a list of coordinates for each star, and **tiny3** will integrate the **tiny2** PSF onto those locations in a single image.

The Tiny Tim distorted PSF represents the image as it would be seen in the raw data frame. Typically, ACS images are undistorted by the data pipeline on the ground. This is usually done by combining observations taken at small offsets (dithers) from each other via a pixel mapping algorithm that includes distortion effects. The interpolated result thus depends on the dithering sequence and interpolation settings used by the software. Because of these observation-dependent parameters, Tiny Tim does not try to replicate the distortion correction done by the pipeline. This complicates life for those modeling ACS, as they must either work with the undistorted data or insert Tiny Tim PSFs into their raw data before distortion correction.

Field dependent aberrations and charge diffusion

The WFC and HRC field-dependent aberrations and charge diffusion variations have been well characterized by phase retrieval (model fitting) analyses of star cluster images[10]. The aberrations and charge diffusion kernels are computed in Tiny Tim base on the field position provided by the user. The WFC charge diffusion varies considerably over the field due to thickness variations in the CCD substrates. The effects are wavelength dependent as well. Due to the undersampling of the PSF in the WFC, charge diffusion is the primary cause of field-dependences in the PSF core width.

Kernels 3 × 3 pixels in size representing the blurring from charge diffusion at the center of the field of each camera at three wavelengths (400, 600, 800 nm) were derived from the phase retrieval analyses. Tiny Tim convolves the distorted image with a new kernel generated by interpolating these three kernels over wavelength. The field dependence of the charge diffusion is implemented as an additional blurring by convolving the image with a Gaussian kernel whose width is computed using the field position specified by the user.

Focus, astigmatism, and coma vary with field position as well, and they are included. The two WFC detectors are also not exactly co-planar, so the resulting focus difference is included.

HRC long-wavelength artifacts

The ACS HRC chip had a defect that creates a halo surrounding the PSF at wavelengths >600 nm. The relative proportion of flux within this halo increases with wavelength. The halo was large (many arcseconds) and contained 10-20% of the total flux. It was caused by the CCD becoming transparent to long wavelength photons, allowing red light to pass through into the glass backing, bounce around, and bounce back into the substrate. The WFC CCDs have a metallized backing that prevents such halo formation. An estimate of the halo is added to all HRC PSFs for wavelengths > 600 nm, however the current halo model is rather poor. There were also diffraction-like spikes that appear at very red wavelengths due to scatter from the electrode structure in the CCD. These are not modeled by Tiny Tim.

7.2 Wide Field Camera 3 (WFC3)

WFC3 is the newest HST camera, and it has two selectable channels: a UV/optical CCD camera (UVIS:f/32, 0.04”/pixel) with two 4096 × 2048 detectors operating at $\lambda = 200 – 1000$ nm and a near-IR HgCdTe camera (IR:f/11.9, 0.13”/pixel) at $\lambda = 800 – 1700$ nm. A variety of narrow-to-wide band filters are available.

Like ACS, WFC3 has significant geometric field distortion. The distorted PSF is computed by **tiny3** for the user-specified detector coordinates. Field dependent aberrations are included using pre-launch relations derived from ray tracing[2]. A wavelength-dependent charge diffusion kernel is used, but the field dependence has not yet been characterized.

The IR channel has a cold stop that masks the warm HST secondary and spider obscurations (but not the primary mirror pads). This is included in Tiny Tim.

8. APPLICATIONS OF TINY TIM

A gauge of the utilization of Tiny Tim is the total of 334 citations (at the time of writing) of a few conference proceeding papers on the software[9,11-13] (a similar estimated number of authors cite the manual or make no reference). The HST community has found a variety of uses for the Tiny Tim PSFs, ranging from instrument calibration (photometric aperture corrections), deconvolution, model convolution, PSF fitting photometry and astrometry, and PSF subtraction.

8.1 Deconvolution

Tiny Tim was initially developed to provide PSFs for deconvolution of spherically aberrated images. Prior to 1995, when new optical error maps were included, the aberrated model PSFs were poor matches to the observed ones. The extended wings were very sensitive to errors in focus, optical surface maps, and obscuration patterns. In some cases, though, Tiny Tim PSFs were all that was available. Note that use of deconvolution is also not limited to spherically aberrated images.

Some examples: Storrs et al.[14] used the subsampling function of Tiny Tim together with deconvolution to restore WF/PC-1 images of asteroids with finer sampling than the originals, showing that the bodies were resolved by HST. Grillmair[15] et al. used models to deconvolve WF/PC-1 images of the central region of the galaxy M51 to reveal structures near the nucleus while Kepner et al.[16] used them to deconvolve WF/PC-1 images to reveal structures in the jet emitted from the young star DG Tauri. Using deconvolution to gain back some resolution on the corrected but undersampled WFPC2 camera images, Burrows et al.[17] showed that the jet of the young star HH 30 narrows as it is seen closer to the star. In a separate paper, Burrows et al.[18] used deconvolution with Tiny Tim PSFs to more clearly reveal the rings around of Supernova 1987a in WFPC2 images (Figure 7).

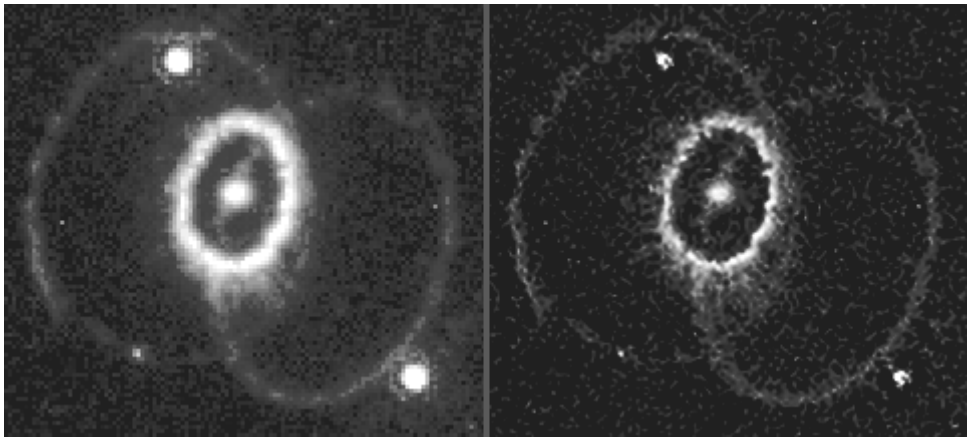

Figure 7. (Left) Image of the remnants of Supernova 1987a observed with the WFPC2 PC in filter F656N. (Right) Result of deconvolving the image with a Tiny Tim model PSF. The nebular rings are better separated from the background stars and the bright ring around the supernova remnant is better defined.

8.2 Image modeling and PSF fitting

Sometimes it is useful to fit PSF-convolved, parameter-constrained models to data, in effect creating a synthetic image. This is essentially the opposite of deconvolution, which may introduce artifacts and is never guaranteed to produce a unique solution. It may involve a model of an extended, resolved component (a galaxy or circumstellar disk) plus, if present, an unresolved component (compact galactic nucleus or star). It may also model one or more stars or unresolved, star-like galactic nuclei. Using Tiny Tim PSFs in this case provides important advantages over using observed ones. PSF models are noiseless, and they can be generated at finer-than-normal sampling. If a subsampled scene is convolved with a subsampled PSF (plus a subsampled PSF added to represent an unresolved source), then the result can be shifted via interpolation and then rebinned to normal sampling. Often this procedure is wrapped in an iterative loop that changes parameters and compares the result to the data until convergence is achieved. Scene generation is typically used to disentangle extended structure of known or assumed spatial distribution (i.e., constrained by an analytical model) from a point source (e.g., galactic nucleus). Misgeld et al.[22], Kim et al.[23], and Matthews et al.[24] used Tiny Tim PSFs and analytical galaxy models to determine distribution parameters for selected galaxies (this appears to be the most popular use of Tiny Tim PSFs). In a similar manner Lamy et al.[25] did the same for the dust surrounding the nuclei of comets. Burrows et al.[17] convolved circumstellar disk models to compare with WFPC2 images of the disk around the infant star HH 30.

One application of image modeling is PSF fitting photometry, which can provide better results than aperture photometry when signal levels are low or the PSFs of multiple stars are blended. Most PSF fitting packages use either analytical models of the PSF (a Gaussian, for instance) or derive a model PSF based on star images in the field. The HST PSF is definitely not Gaussian in shape, even in the core, and many HST images do not have sufficient stars to create an empirical PSF model (and one that is not as finely sample as a Tiny Tim model can be). An example of model PSF fitting is shown in Figure 8, a WFPC2 PC image of the binary star XZ Tauri[19]. A Tiny Tim subsampled PSF was generated and used in a nonlinear least squares optimizer to create a synthetic binary image, with the PSF offsets and fluxes derived. The aberration parameters of the PSF itself (focus, coma) were iteratively optimized to provide the best match (something that cannot be done if using observed PSFs from other epochs). Similar analyses have been done by others[20]. Dolphin[21] has created a stellar photometry package for WFPC2 that utilized Tiny Tim PSFs. Using models, it is possible to determine the position of a star within about 0.01 pixel.

Related to PSF fitting is PSF subtraction (one must fit the PSF with something before subtracting it). It is used to remove the entire PSF of an unresolved source (star, galaxy nucleus) so that faint objects can be seen. Figure 9 shows the Tiny Tim PSF fits from Figure 8 scaled to a long exposure image of the same system and subtracted to remove the halo of light, more clearly revealing the outflow from the stars. For subtraction in the wings, usually an observed reference PSF provides superior results than using a model, as the match to the fine scale structure is better. In this example, however,

the object was located near the edge of the field and no suitable observed PSFs were available. A halo of subtraction residuals may be seen, but the improvement in contrast is still useful.

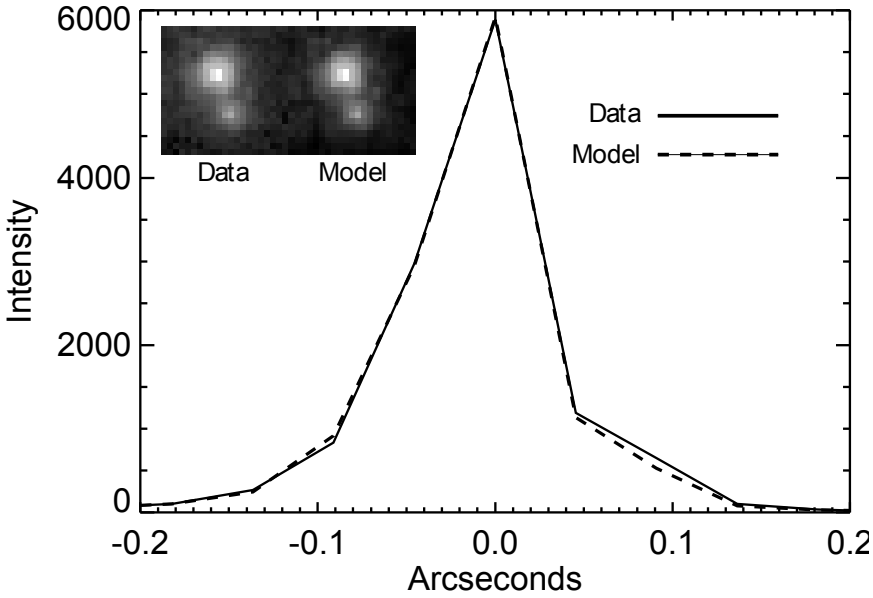

Figure 8. (Inset) Short exposure image of the 0.3" separation binary star XZ Tauri imaged with the WFPC2 PC camera (0.0455"/pixel). Two copies of a subsampled Tiny Tim PSF model were fit to the data using an iterative, non-linear solver to match positions and intensities to create a synthetic binary model. (Plot) A horizontal cross section through the brighter star.

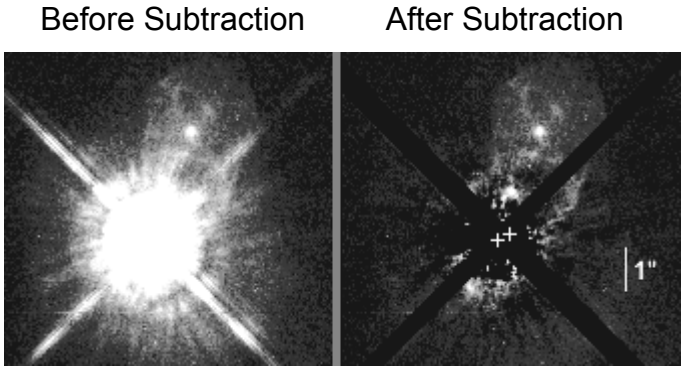

Figure 9. (Left) Long exposure image of the XZ Tauri binary system using WFPC2 PC and filter F675W. An outflow from the system is seen extending to the upper right, but the glare of the PSFs interfere with details closer to the stars. (Right) The image after subtraction of two Tiny Tim PSFs matched to the stars. The diffraction spike residuals have been masked.

9. TINY TIM FOR SPITZER

The success of Tiny Tim for HST lead to the development of a version for the Spitzer Space Telescope, developed by J. Krist under contract to the Spitzer Science Center. Much of the same functionality exists in the Spitzer version, but with new features specifically for the infrared (λ = 3 – 160 μm) telescope. The Spitzer telescope obscuration pattern, for instance, is field dependent because the secondary mirror is supported by vanes extending from the center of the primary. The stellar spectra were replaced with blackbody and power law options.

10. SUMMARY

Tiny Tim has been the standard source for HST PSF models for the past 20 years. Its acceptance by the astronomical community has been due to its ease of use, portability, speed, and incorporation of measured HST parameters. It has continued to be updated throughout its history, adding new cameras and measured characteristics. Now that Hubble is entering its final years with no additional servicing missions, no new cameras will be installed. Sometime in this decade it will likely cease functioning. However, there will always be an enormous archive of data that astronomers will analyze for decades to come, so Tiny Tim will likely continue to serve its purpose for just as long.

ACKNOWLEDGEMENTS

Tiny Tim for HST is currently being maintained at STScI by Matthew Lallo and Todd Miller. The authors thank all those who provided information, bug fixes, and suggestions over the years, including (but definitely not limited to) Hashima Hasan, Christopher Burrows, Russ Makidon, Matthew Lallo, George Hartig, Stefano Casertano, Marco Sirianni, Jon Holtzman, Tom Brown, and Colin Cox.

REFERENCES

[1] Hasan, H., and Burrows, C., "Telescope Image Modeling (TIM)", Pub. Astronomical Soc. of the Pacific 107, 289 (1995).
[2] Hook, R., and Stoehr, F., "WFC3 Support in Tiny Tim", STScI Instrument Science Report WFC3-2008-014 (available from www.stsci.edu/hst) (2008).
[3] Krist, J., and Burrows, C., "Phase retrieval analysis of pre- and post-repair Hubble Space Telescope images", Applied Optics 34, 4951 (1995).
[4] Makidon, R., Lallo, M., Casertano, S., Gilliland, R., Sirianni, M., and Krist, J., "The temporal optical behavior of the Hubble Space Telescope: the impact on science observations", Proc. SPIE 6270, 62701L (2006).
[5] Lallo, M., Makidon, R., Casertano, S., and Krist, J., "Temporal optical behavior of HST: focus, coma, and astigmatism history", Proc. SPIE 6270, 62701N (2006).
[6] Cox., C., and Niemi, S.-M., "Evaluation of a temperature-based HST focus model", STScI Instrument Science Report TEL-1011-01 (available from www.stsci.edu/hst) (2011).
[7] Burrows, C., Holtzman, J., Faber, S., Bely, P., Hasan, H., Lynds, C., and Schroeder, D., "The imaging performance of the Hubble Space Telescope", Astrophysical Journal Letters 369, 21 (1991).
[8] T. Lauer, "The Photometry of Undersampled Point-Spread Functions", Pub. Astronomical Soc. of the Pacific 111, 1434 (1999).
[9] Krist, J., and Hook, R., "NICMOS PSF variations and Tiny Tim simulations", Proc. of the 1997 HST Calibration Workshop, 192 (1997).
[10] Krist, J., "Position-dependent CCD charge diffusion: results from HST/ACS", Proc. SPIE 5499, 328 (2004).
[11] Krist, J., "Tiny Tim: an HST PSF Simulator", Proc. Astronomical Data Analysis Software and Systems II., A.S.P. Conference Series 52, 536 (1993).
[12] Krist, J., "Simulation of HST PSFs using Tiny Tim", Proc. Astronomical Data Analysis and Software Systems IV., A.S.P. Conference Series 77, 349 (1995).
[13] Krist, J., and Hasan, H., "Deconvolution of HST WFPC Images using Simulated Images", Proc. Astronomical Data Analysis and Software Systems II., A.S.P. Conference Series 52, 530 (1993).
[14] Storrs, A., Dunne, C., Conan, J.-M., Mugnier, L., Weiss, B. P., and Zellner, B., "A closer look and main belt asteroids 1: WF/PC images", Icarus 173, 409 (2005).
[15] Grillmair, C., Faber, S., Lauer, T., Hester, J., Lynds, C., and O'Neil, E., "The Nuclear Region of M51 Imaged with the HST Planetary Camera", Astronomical Journal 113, 225 (1997).
[16] Kepner, J., Hartigan, P., Yang, C., and Strom, S., "Hubble Space Telescope Images of the Subarcsecond Jet in DG Tauri", Astrophysical Journal Letters 415, 119 (1993).
[17] Burrows, C., et al., "Hubble Space Telescope Observations of the Disk and Jet of HH 30", Astrophysical Journal 473, 437 (1996).
[18] Burrows, C., Krist, J., Hester, et al., "Hubble Space Telescope Observations of the SN 1987A Triple Ring Nebula", Astrophysical Journal 452, 680 (1995).

[19] Krist, J., et al., "Hubble Space Telescope WFPC2 Imaging of XZ Tauri: Time Evolution of a Herbig-Haro Bow Shock", Astrophysical Journal Letters 515, 35 (1999).
[20] Burgasser, Adam J.; Bardalez-Gagliuffi, Daniella C.; Gizis, John E., "Hubble Space Telescope Imaging and Spectral Analysis of Two Brown Dwarf Binaries at the L Dwarf/T Dwarf Transition", Astronomical Journal, 141, 70 (2011).
[21] Dolphin, A. E., "WFPC2 Stellar Photometry with HSTPHOT", Pub. of the Astronomical Soc. of the Pacific, 112, 1383 (2000).
[22] Misgeld, I., Mieske, S., Hilker, M., Richtler, T., Georgiev, I. Y., and Schuberth, Y., "A large population of ultra-compact dwarf galaxies in the Hydra I cluster", Astronomy & Astrophysics, 531, 4 (2011).
[23] Kim, M., Ho, L., Peng, C., Barth, A., and Im, M., "Decomposition of the Host Galaxies of Active Galactic Nuclei Using Hubble Space Telescope Images", Astrophysical Journal Supplement, 179, 283 (2008).
[24] Matthews, L., et al., "WFPC2 Observations of Compact Star Cluster Nuclei in Low-Luminosity Spiral Galaxies", Astronomical Journal 118, 208 (1999).
[25] Lamy, P., Toth, I., Weaver, H., A'Hearn, M., and Jorda, L., "Properties of the nuclei and comae of 10 ecliptic comets from Hubble Space Telescope multi-orbit observations", Monthly Notices of the Royal Astronomical Society, 412, 1573 (2011).